Frontiers of Information Technology & Electronic Engineering
www.jzus.zju.edu.cn; engineering.cae.cn; www.springerlink.com
ISSN 2095-9184 (print); ISSN 2095-9230 (online)
E-mail: jzus@zju.edu.cn

Beam squint effect on high-throughput millimeter-wave communication with an ultra-massive phased array*

Zhiqiang WANG, Jiawei LIU, Jun WANG, Guangrong YUE‡

National Key Laboratory of Science and Technology on Communications, University of Electronic Science and Technology of China, Chengdu 611731, China

E-mail: wangzq@std.uestc.edu.cn; 842927584@qq.com; junwang@uestc.edu.cn; yuegr@uestc.edu.cn

Received Sept. 2, 2020; Revision accepted Feb. 9, 2021; Crosschecked Mar. 3, 2021

Abstract: An ultra-massive phased array can be deployed in high-throughput millimeter-wave (mmWave) communication systems to increase the transmission distance. However, when the signal bandwidth is large, the antenna array response changes with the frequency, causing beam squint. In this paper, we investigate the beam squint effect on a high-throughput mmWave communication system with the single-carrier frequency-domain equalization transmission scheme. Specifically, we first view analog beamforming and the physical channel as a spatial equivalent channel. The characteristics of the spatial equivalent channel are analyzed which behaves like frequency-selective fading. To eliminate the deep fading points in the spatial equivalent channel, an advanced analog beamforming method is proposed based on the Zadoff-Chu (ZC) sequence. Then, the low-complexity linear zero-forcing and minimum mean squared error equalizers are considered at the receiver. Simulation results indicate that the proposed ZC-based analog beamforming method can effectively mitigate the performance loss by the beam squint.

Key words: Ultra-massive phased array; Millimeter-wave (mmWave); Beam squint; Zadoff-Chu; Single-carrier frequency-domain equalization (SC-FDE)

https://doi.org/10.1631/FITEE.2000451 **CLC number:** TN928

1 Introduction

With the numerous available spectra in the millimeter-wave (mmWave) bands ranging from 30 to 300 GHz, high-throughput mmWave communication has been regarded as a key enabling technology for fifth-generation (5G) cellular networks and beyond, which can support extremely high data rate wireless transmissions (Roh et al., 2014; Sun et al., 2014; Swindlehurst et al., 2014; Hemadeh et al., 2018). However, the effective communication distance is limited by the severe signal attenuation at mmWave frequencies. Fortunately, thanks to the smaller size of antennas at higher frequencies, mmWave systems allow a large number of antennas to be packed into a small area to provide significant beamforming gains to compensate for the severe attenuation (Heath et al., 2016; Kutty and Sen, 2016; Busari et al., 2018). Despite many benefits of mmWave communication using an ultra-massive antenna array, there are still numerous challenges to fully obtain the advantages of an ultra-massive antenna array when simultaneously considering the system performance and complexity.

Considering long-range point-to-point line-of-sight (LoS) high-throughput mmWave communication scenarios (e.g., wireless backhaul, inter-aircraft data link, and space satellite communication), a simple ultra-massive phased array (i.e., pure analog beamforming) can be deployed in mmWave systems, and forms single narrow beam to establish a

‡ Corresponding author

* Project supported by the National Key R&D Program of China (No. 2020YFB1805001), the National Natural Science Foundation of China (No. 61831004), and the Defense Industrial Technology Development Program, China (No. JCKY2016204A603)

ORCID: Zhiqiang WANG, https://orcid.org/0000-0001-6398-5298; Guangrong YUE, https://orcid.org/0000-0001-7937-124X

robust communication link. In this architecture, all antenna elements are connected via a phase shifter network to a radio frequency (RF) chain. However, when the number of antennas and the signal bandwidth are large, the physical propagation delay of electromagnetic wave across the ultra-massive array aperture can be comparable with the symbol period. Thus, the time delay between antenna elements for a baseband signal cannot be ignored, and causes the antenna array response to be frequency-dependent. However, note that the value of the phase shifter is frequency-independent in the ultra-massive phased array. This leads to the beam squint phenomenon: the formed beam direction varies with frequency when the narrowband standard beamforming method is used in the wideband case (Mailloux, 2005), which limits the effective operating bandwidth of the phased array and leads to poor performance in wideband systems.

Although the true time delay (TTD) based array (Rotman et al., 2016) or full-digital (FD) array (Liu W and Weiss, 2010) can be used to mitigate beam squint, where the realized beamforming weight is frequency-dependent, the TTD-based array and FD array have higher implementation cost and higher power consumption than the phased array, making them unsuitable for high-throughput mmWave ultra-massive antenna array systems. Recently, the effect of beam squint on a mmWave communication system has received attention. Cai et al. (2016) analyzed the influence of beam squint on codebook design for analog beamforming in mmWave systems. Brady and Sayeed (2015) proposed a novel beamspace receiver for wideband mmWave systems to reduce the performance loss by beam squint. A semidefinite relaxation (SDR) based beam optimization technique was developed in Liu XM and Qiao (2019). In our previous work (Wang ZQ et al., 2018), a digital baseband compensation method was proposed to eliminate the beam squint effect.

In addition to the reduced beamforming gain caused by the beam squint phenomenon, beam squint causes the communication channel to appear as a frequency-selective channel even in an LoS wireless channel, where the symbol is expanded to multiple times, and the delayed replicas of previous symbols interfere with the current symbol, i.e., inter-symbol interference (ISI). Moreover, the performance loss due to ISI cannot be eliminated by increasing the transmission power (Tse and Viswanath, 2005). Traditionally, to avoid or mitigate ISI in the wideband frequency-selective channel, there are two practical modulation schemes (Falconer et al., 2002; Wang ZD et al., 2004), i.e., orthogonal frequency-division multiplexing (OFDM) and single-carrier (SC) modulation with receiver equalization. In the OFDM modulation scheme, multiple modulated subcarriers are transmitted in parallel and each subcarrier occupies only a very narrow bandwidth. Because only the amplitude and phase of each subcarrier are affected by the channel distortions, the compensation of frequency-selective fading is performed at each sub-channel. In the SC modulation scheme, the ISI is mitigated at the receiver by using different equalization algorithms. By contrast, the single-carrier frequency-domain equalization (SC-FDE) scheme has similar performance compared with the OFDM modulation scheme. Moreover, the SC-FDE modulation scheme has a lower peak-to-average power ratio (PAPR) and reduced sensitivity to carrier frequency offsets than the OFDM modulation scheme. Thus, the SC-FDE modulation scheme is a more attractive modulation scheme for high-throughput mmWave communication systems (Wu et al., 2016; Buzzi et al., 2018). With the OFDM modulation scheme, some channel estimation and beamforming algorithms have been proposed (Liu B et al., 2018; Rodriguez-Fernandez and Gonzalez-Prelcic, 2018; González-Coma et al., 2019), considering the beam squint effect in ultra-massive antenna array systems. However, there are few studies of the beam squint effect on high-throughput mmWave SC-FDE systems.

In this study, we investigate the beam squint effect on a high-throughput mmWave communication system with the SC-FDE transmission scheme. The contributions can be summarized as follows:

1. Characteristic analysis of the spatial equivalent channel

From a communication perspective, the antenna array response of a uniform linear array (ULA) and the standard analog beamforming vector are modeled as a spatial equivalent channel in high-throughput mmWave LoS multiple-input single-output (LoS-MISO) systems. We observe that beam squint causes obvious beamforming gain loss. Moreover, when the signal bandwidth and the number of antennas are large, the spatial equivalent

channel is a frequency-selective channel, in which multiple deep fading points exist.

2. Zadoff-Chu (ZC) based analog beamforming method

We propose an advanced analog beamforming method based on the ZC sequence to eliminate the deep fading points of the spatial equivalent channel. With linear zero-forcing (ZF) and minimum mean squared error (MMSE) frequency-domain equalizers at the receiver, the bit-error-rate (BER) performance of a high-throughput mmWave SC-FDE system is simulated to demonstrate the beam squint effect on system performance and verify the effectiveness of the proposed beamforming method.

Notations used throughout the paper are as follows: Superscripts $(\cdot)^{\mathrm{T}}$, $(\cdot)^{\mathrm{H}}$, and $(\cdot)^{-1}$ stand for the transpose, conjugate-transpose, and inversion of a matrix or a vector, respectively. $\boldsymbol{A} \odot \boldsymbol{B}$ denotes the Hardmard product of $\boldsymbol{A}$ and $\boldsymbol{B}$. $E[\cdot]$ denotes the expectation operator.

2 Wideband beam squint phenomenon in an ultra-massive phased array

As depicted in Fig. 1, we consider an LoS-MISO system where the transmitter (TX) is equipped with an N-dimensional ULA and the receiver (RX) deploys a single antenna. At the TX, the antenna spacing in the ULA is d. The carrier signal wavelength is λ_{c}, corresponding to the signal carrier frequency $f_{\mathrm{c}} = c/\lambda_{\mathrm{c}}$, where c is the wave propagation velocity. In general, the antenna spacing is selected as $d = \lambda_{\mathrm{c}}/2$. The transmitted baseband modulated signal $s(t)$ can be represented as

$$s(t) = \sum_{i=-\infty}^{+\infty} s[i]C(t - iT_{\mathrm{sys}}), \tag{1}$$

where $s[i]$ is the transmitted symbol with symbol period T_{sys}, and the symbol rate is $f_{\mathrm{sys}} = 1/T_{\mathrm{sys}}$. $C(t)$ is the raised cosine filter function with the roll-off factor $\alpha \in [0,1]$. The signal bandwidth of $s(t)$ is $B = (1+\alpha)f_{\mathrm{sys}}$, and we consider that the communication channel is a band-limited channel with bandwidth B. The average power of the transmitted signal $s(t)$ is P. The RF front end is composed of a single RF chain and a network of N phase shifters at the TX. By configuring the phase shifters in the phased array, the TX can direct its RF signals to maximize signal power at the receiver. The transmitted equivalent baseband time-domain signal of the n^{th} antenna element can be expressed as

$$r_n(t) = s(t-\tau_n)\mathrm{e}^{-\mathrm{j}2\pi f_{\mathrm{c}}\tau_n + \phi_n} = h_n(t) \otimes s(t), \tag{2}$$

where n $(n = 0, 1, \ldots, N-1)$ is the antenna index, $\tau_n = n\tau$ is the time delay between the n^{th} antenna and the reference antenna, and $\tau = d\sin\theta/c$ denotes the time delay between the adjacent antennas with $\theta \in [-\pi/2, \pi/2]$ the angle of departure (AoD) parameter of a physical LoS-MISO channel. Here, we choose the first antenna as the reference antenna. The reference antenna index is $n = 0$. The phase ϕ_n denotes the value of the n^{th} phase shifter. $h_n(t)$ denotes the equivalent time-domain impulse response of the n^{th} antenna, and "$\otimes$" is the convolution operation. From Eq. (2), we can observe that the antenna response can be decomposed into two parts, in which the first part $s(t-\tau_n)$ is the time delay version of the equivalent baseband signal $s(t)$, and the second part $\mathrm{e}^{-\mathrm{j}2\pi f_{\mathrm{c}}\tau_n}$ is the response to the carrier signal.

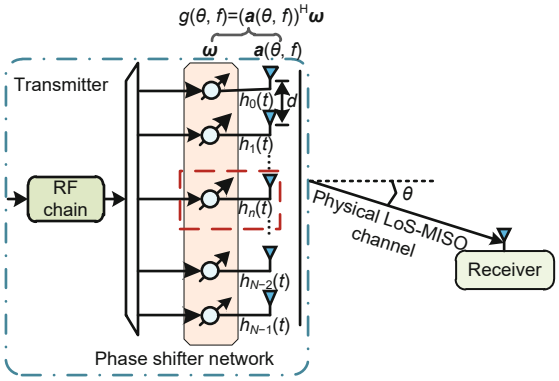

Fig. 1 Model of a line-of-sight multiple-input single-output (LoS-MISO) system where the transmitter deploys an ultra-massive phased array

At the RX, ignoring the signal attenuation in free space, the received signal can be written as

$$y(t) = \sum_{n=0}^{N-1} r_n(t) + n(t) = h(t) \otimes s(t) + n(t), \tag{3}$$

where

$$h(t) = \sum_{n=0}^{N-1} h_n(t) = \left[\boldsymbol{a}(\theta) \odot \boldsymbol{\Theta}(t)\right]^{\mathrm{T}} \boldsymbol{w}, \tag{4}$$

$$\boldsymbol{a}(\theta) = \left[\mathrm{e}^{-\mathrm{j}2\pi f_{\mathrm{c}}\tau_0}, \mathrm{e}^{-\mathrm{j}2\pi f_{\mathrm{c}}\tau_1}, \ldots, \mathrm{e}^{-\mathrm{j}2\pi f_{\mathrm{c}}\tau_{N-1}}\right]^{\mathrm{T}}, \tag{5}$$

$$\boldsymbol{\Theta}(t) = \left[\delta(t-\tau_0), \delta(t-\tau_1), \ldots, \delta(t-\tau_{N-1})\right]^{\mathrm{T}}, \tag{6}$$

$$\boldsymbol{w} = \left[\mathrm{e}^{\mathrm{j}\phi_0}, \mathrm{e}^{\mathrm{j}\phi_1}, \ldots, \mathrm{e}^{\mathrm{j}\phi_{N-1}}\right]^{\mathrm{T}}, \tag{7}$$

$n(t)$ denotes the complex Gaussian white noise with the power σ^2, and we define the signal-to-noise ratio (SNR) as P/σ^2 in this study. $\delta(\cdot)$ is the Dirac impulse function. Actually, $h(t)$ represents the time-domain response of the spatial equivalent channel, $\boldsymbol{w}$ denotes the analog beamforming vector, $\boldsymbol{\Theta}(t)$ represents the time delay for the equivalent baseband signal $s(t)$, and $\boldsymbol{a}(\theta)$ denotes the antenna array response to the carrier signal, which is often known as the narrowband array response vector. When the number of antennas N and the signal bandwidth of $s(t)$ are small, the time delay for the equivalent baseband signal on each antenna element can be ignored, i.e., $s(t-\tau_n)\approx s(t),\ n=0,1,\ \ldots,\ N$. Based on the above narrowband assumption, $h(t)$ degenerates to $h(t)=\left[(\boldsymbol{a}(\theta))^{\mathrm{T}}\boldsymbol{w}\right]\delta(t)$, and Eq. (3) is simplified as $y(t)=\left[(\boldsymbol{a}(\theta))^{\mathrm{T}}\boldsymbol{w}\right]s(t)+n(t)$, which is the narrowband array signal processing model.

Inversely, when the number of antennas N or the signal bandwidth is large, the narrowband assumption does not hold, making the traditional narrowband array signal processing model invalid. In this case, we transform the received signal $y(t)$ to the frequency domain, which can be expressed as

$$y(f)=\left[(\boldsymbol{a}(\theta,f))^{\mathrm{T}}\boldsymbol{w}\right]s(f)+n(f), \tag{8}$$

where

$$\begin{aligned}\boldsymbol{a}(\theta,f)=&\left[\mathrm{e}^{-\mathrm{j}2\pi(f+f_{\mathrm{c}})\tau_0},\mathrm{e}^{-\mathrm{j}2\pi(f+f_{\mathrm{c}})\tau_1},\right.\\&\left.\ldots,\mathrm{e}^{-\mathrm{j}2\pi(f+f_{\mathrm{c}})\tau_{N-1}}\right]^{\mathrm{T}},\end{aligned} \tag{9}$$

f is within the range $[-B/2,\ B/2]$, and $s(f)$ and $n(f)$ denote the frequency-domain expressions of $s(t)$ and $n(t)$, respectively. Eq. (8) is the frequency-domain wideband array signal model, and $\boldsymbol{a}(\theta,f)$ is the wideband array response vector in the frequency domain. It holds that $\boldsymbol{a}(\theta,f)=\boldsymbol{a}(\theta)$ when $f=0$. Obviously, the antenna array response vector is no longer dependent on the AoD parameter θ alone, but also depends on the frequency f, which is the critical difference between the narrowband and wideband array signal processing.

Next, we describe the beam squint phenomenon in an ultra-massive phased array when conventional standard beamforming is used (Mailloux, 2005). The goal of beamforming in a phased array is to adjust the values of phase shifters to achieve directional transmission and maximize the received signal power. However, note that the value of the phase shifter is unrelated to the frequency. In the conventional standard analog beamforming method, the value of the phase shifter is designed based on the carrier frequency f_{c}. Assuming that the expected beam direction is θ_0, the analog beamforming vector with power normalization is

$$\boldsymbol{w}_{\mathrm{std}}=\frac{1}{\sqrt{N}}\left[\mathrm{e}^{\mathrm{j}\phi_{\mathrm{std},0}},\mathrm{e}^{\mathrm{j}\phi_{\mathrm{std},1}},\ldots,\mathrm{e}^{\mathrm{j}\phi_{\mathrm{std},N-1}}\right]^{\mathrm{T}}, \tag{10}$$

where

$$\phi_{\mathrm{std},n}=2\pi f_{\mathrm{c}}n\frac{d\sin\theta_0}{c},\ n=0,1,\ \ldots,\ N-1. \tag{11}$$

In the wideband case, the antenna array response vector $\boldsymbol{a}(\theta,f)$ has two independent variables, i.e., the AoD parameter θ and the frequency f. If the beamforming vector $\boldsymbol{w}_{\mathrm{std}}$ is used, the corresponding beam pattern function can be expressed as

$$\begin{aligned}g(\boldsymbol{w}_{\mathrm{std}},\theta,f)&=(\boldsymbol{a}(\theta,f))^{\mathrm{T}}\boldsymbol{w}_{\mathrm{std}}\\&=\frac{1}{\sqrt{N}}\sum_{n=0}^{N-1}\mathrm{e}^{-\mathrm{j}2\pi n\frac{d}{c}[(f+f_{\mathrm{c}})\sin\theta-f_{\mathrm{c}}\sin\theta_0]}\\&=\frac{1}{\sqrt{N}}\mathrm{e}^{-\mathrm{j}(N-1)\pi\frac{d}{c}[(f+f_{\mathrm{c}})\sin\theta-f_{\mathrm{c}}\sin\theta_0]}\\&\quad\cdot\underbrace{\frac{\sin\left\{N\pi\frac{d}{c}[(f+f_{\mathrm{c}})\sin\theta-f_{\mathrm{c}}\sin\theta_0]\right\}}{\sin\left\{\pi\frac{d}{c}[(f+f_{\mathrm{c}})\sin\theta-f_{\mathrm{c}}\sin\theta_0]\right\}}}_{D\left(\frac{d}{c}[(f+f_{\mathrm{c}})\sin\theta-f_{\mathrm{c}}\sin\theta_0]\right)},\end{aligned} \tag{12}$$

where $D(x)=\dfrac{\sin(\pi Nx)}{\sin(\pi x)}$ is the Dirichlet sinc function with $x=\dfrac{d}{c}[(f+f_{\mathrm{c}})\sin\theta-f_{\mathrm{c}}\sin\theta_0]$. Note that the maximum value of $g(\boldsymbol{w}_{\mathrm{std}},\theta,f)$ is obtained when $x=0$, and the corresponding beam direction is

$$\theta_{\max}(f)=\arcsin\left(\frac{\sin\theta_0}{1+f/f_{\mathrm{c}}}\right), \tag{13}$$

indicating that the exact beam direction formed by the phased array varies with the frequency in the wideband case, i.e., the beam squint phenomenon. As a special case, beam squint does not exist when $\theta_0=0$. Fig. 2 plots the beam pattern $|g(\boldsymbol{w},\theta,f)|$ at the frequency $f=-0.0330f_{\mathrm{c}},\ -0.0165f_{\mathrm{c}},\ 0,\ 0.0165f_{\mathrm{c}}$, and $0.0330f_{\mathrm{c}}$ with $N=256$ and $\theta_0=10^\circ$ to illustrate the beam squint phenomenon. We can see that the maximum beamforming gain is obtained only at the carrier frequency ($f=0$), and the beamforming gains at all other frequencies are smaller

than that at the carrier frequency in the expected beam direction, as shown in the right subfigure of Fig. 2. Moreover, the beam offset angle by beam squint is determined by the expected beam direction θ_0 and the signal bandwidth B. The antenna number N has no impact on the beam direction changing characteristics. However, the larger the number of antenna elements N, the smaller the beamwidth, and the beamforming gain of the different frequency at the expected beam direction decreases rapidly with a little beam squint. Thus, the beam squint on system performance is determined by three parameters: signal bandwidth B, beam direction θ_0, and antenna number N.

3 Spatial equivalent channel in an LoS-MISO system and the proposed ZC-based analog beamforming

In Section 2, the wideband beam squint phenomenon in an ultra-massive phased array with the standard analog beamforming has been discussed. However, it cannot directly reflect the beam squint effect on high-throughput mmWave communication systems. In this section, we further consider beam squint from a communication perspective, where the analog beamforming and the physical LoS-MISO channel are viewed as a spatial equivalent channel, and the characteristics of the spatial equivalent channel are analyzed. Then, a novel analog beamforming method is proposed based on the ZC sequence to improve the quality of the spatial equivalent channel and mitigate, to some extent, the system performance loss caused by the beam squint phenomenon.

3.1 Spatial equivalent channel

In the considered LoS-MISO system, the transmitted signal is assigned to multiple array channels via a phase shifter network and then transmitted to the RX. Note that the analog beamforming vector $\boldsymbol{w}_{\mathrm{std}}$ can eliminate only the spatial phase difference of each antenna at the carrier frequency f_{c}. However, the time delay for the baseband signal still exists. From a communication viewpoint, the physical LoS-MISO channel and the analog beamforming can be viewed as an array multi-path channel, which consists of N antenna sub-channels (N propagation paths). The characteristics of the array multi-path channel are described as follows:

1. Each antenna sub-channel consists of the antenna response and the phase shifter, which is equivalent to a signal propagation path. Correspondingly, the time-domain response of each antenna sub-channel can be expressed as $h_n(t) = \delta(t-\tau_n)\mathrm{e}^{-\mathrm{j}2\pi f_{\mathrm{c}}\tau_n+\phi_n}$.

2. Each signal propagation path (antenna sub-channel) has the same attenuation with different time delay, and the time delay increases linearly with the antenna's index.

We define the time delay of the transmitted

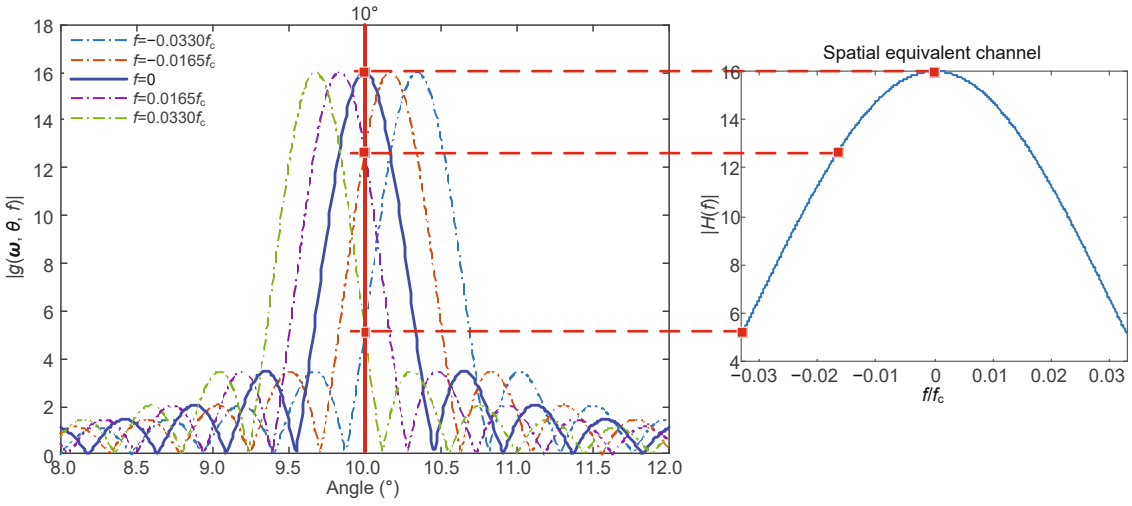

Fig. 2 Beam squint in an ultra-massive phased array with the number of antennas $N = 256$ and the expected beam direction $\theta_0 = 10°$. The right subfigure is the corresponding amplitude frequency response of the spatial equivalent channel in the LoS-MISO system. References to color refer to the online version of this figure

signal between the first antenna (antenna index $n=0$) and the last antenna (antenna index $n=N-1$) as the aperture delay spread, i.e.,

$$\tau_{\max}=|(N-1)\tau|=\left|\frac{(N-1)d\sin\theta}{c}\right|. \tag{14}$$

Actually, the aperture delay spread equals the multi-path delay spread of the wireless channel. From Eq. (14), we can observe that the aperture delay spread depends on the number of antennas N, the antenna spacing d, and the AoD parameter θ. When $d=\lambda_{\mathrm{c}}/2$ and $\theta=\pm\pi/2$ (the worst case), the maximum aperture delay spread is $\tau_{\max\_\mathrm{worst}}=0.5(N-1)/f_{\mathrm{c}}$. In the concerned high-throughput mmWave communication system with an ultra-massive phased array, the number of antennas N and the signal bandwidth B are large; thus, the aperture delay spread $\tau_{\max}$ can be comparable to the symbol period. For instance, for a mmWave communication system at the carrier frequency $f_{\mathrm{c}}=60$ GHz with $N=256$ and $d=\lambda_{\mathrm{c}}/2$, the symbol rate $f_{\mathrm{sys}}=2$ Gsymbol/s, we can obtain the aperture delay spread in the worst case $\tau_{\max\_\mathrm{worst}}=4.26T_{\mathrm{sys}}$. Thus, the time delay for the baseband signal cannot be ignored and the array response $\boldsymbol{a}(\theta,f)$ depends on the signal departure angle θ and the frequency f, and the beam squint effect on the mmWave system must be concerned.

A simple communication system model is shown in Fig. 3, where the forementioned array multi-path channel is referred to as a spatial equivalent channel. The time-domain response of the spatial equivalent channel is described in Eq. (4), and we can also obtain the frequency-domain response $H(f)$, which can be written as

$$H(f)=\left(\boldsymbol{a}(\theta,f)\right)^{\mathrm{T}}\boldsymbol{w}=\sum_{n=0}^{N-1}w_n\mathrm{e}^{-\mathrm{j}2\pi n(f+f_{\mathrm{c}})\frac{d\sin\theta}{c}}, \tag{15}$$

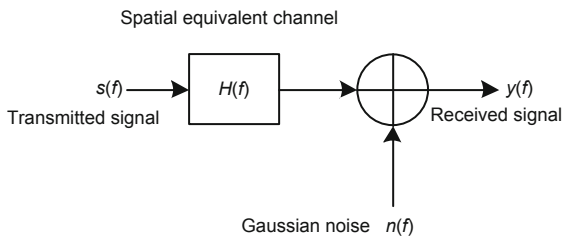

Fig. 3 A simple communication system model with the spatial equivalent channel

where $w_n=\mathrm{e}^{\mathrm{j}\phi_n}$ denotes the n^{th} element of the analog beamforming vector $\boldsymbol{w}$. Assuming that the AoD of the physical LoS-MISO channel is known perfectly at the TX, the standard analog beamforming vector $\boldsymbol{w}_{\mathrm{std}}$ is designed using the perfect AoD, i.e., $\theta_0=\theta$. The frequency-domain response of the spatial equivalent channel in the standard beamforming method can be expressed as

$$\begin{aligned}H_{\mathrm{std}}(f)&=\left(\boldsymbol{a}(\theta,f)\right)^{\mathrm{T}}\boldsymbol{w}_{\mathrm{std}}\\&=\frac{1}{\sqrt{N}}\mathrm{e}^{-\mathrm{j}\pi\frac{d}{c}(N-1)f\sin\theta}\frac{\sin(N\pi\frac{d}{c}f\sin\theta)}{\sin(\pi\frac{d}{c}f\sin\theta)}.\end{aligned} \tag{16}$$

Actually, the frequency-domain response $H_{\mathrm{std}}(f)$ is the value of the beam pattern function $g(\boldsymbol{w}_{\mathrm{std}},\theta,f)$ at θ_0, which reflects the beamforming gain of each frequency at θ_0, as shown in Fig. 2. From Eq. (16), we can see that the properties of the spatial equivalent channel are correlated with the number of antennas N, the AoD of the LoS-MISO channel θ, and the signal bandwidth B. Thus, the spatial equivalent channel can effectively reflect the beam squint effect on the considered mmWave communication system.

Fig. 4 shows the frequency-domain response $H_{\mathrm{std}}(f)$ with $\theta=0°$, $10°$, and $30°$, $N=256$, $f_{\mathrm{c}}=60$ GHz, and $B=4$ GHz. It can be seen that the spatial equivalent channel is no longer an ideal flat channel when $\theta\neq0°$. Moreover, when $\theta=30°$, the spatial equivalent channel is a frequency-selective channel, in which multiple deep fading points exist. In the considered LoS-MISO system, the wireless physical channel only has a single LoS path. So, the frequency-selective characteristic of the spatial equivalent channel is caused only by beam squint, rather than the multi-path effect in a wireless channel. Moreover, the average beamforming gain versus N is plotted in Fig. 5. It can be seen that the beamforming gain does not increase anymore when the number of antennas N exceeds a certain number due to the beam squint effect. So, beam squint will result in obvious beamforming gain loss.

3.2 Proposed ZC-based analog beamforming

Beam squint not only causes the beamforming gain to decrease, but also causes the spatial equivalent channel to become a frequency-selective channel with multiple deep fading points. Here, we propose a novel analog beamforming method based on

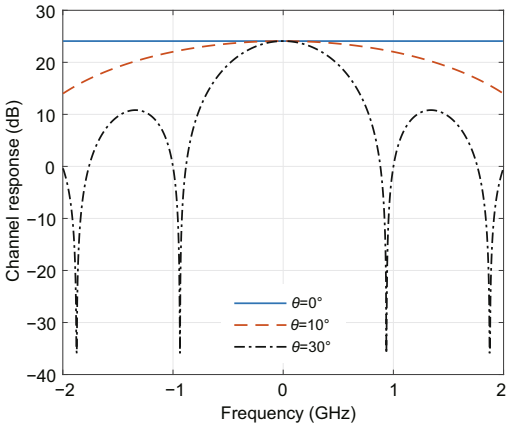

Fig. 4 Frequency-domain response of the spatial equivalent channel in the standard beamforming method with $\theta = 0°$, $10°$, and $30°$ ($N = 256$, $f_c = 60$ GHz)

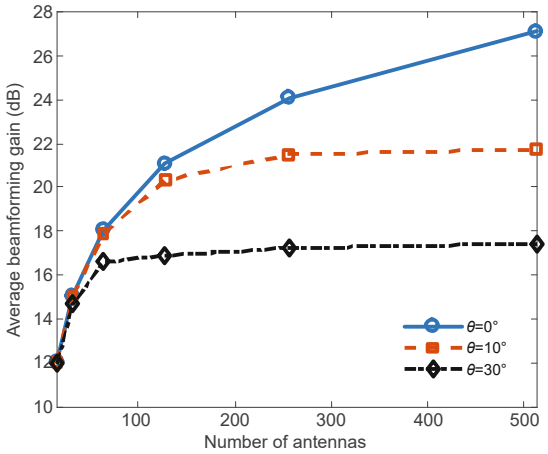

Fig. 5 Average beamforming gain versus the number of antennas N with $\theta = 0°, 10°$, and $30°$ ($B = 4$ GHz, $f_c = 60$ GHz)

the ZC sequence to eliminate the deep fading points caused by beam squint. From Eq. (15), we can see that the frequency-domain response $H(f)$ is actually the discrete Fourier transform (DFT) of the beamforming weight w_n in terms of the antenna index n where $f \in [-B/2,\ B/2]$. Thus, to obtain a frequency-flat spatial equivalent channel, we can design a sequence w_n ($n = 0,\ 1,\ \ldots,\ N-1$), which has a constant magnitude Fourier transform over $f \in [-B/2,\ B/2]$. Furthermore, the sequence w_n ($n = 0,\ 1,\ \ldots,\ N-1$) needs to satisfy the constant amplitude. Note that Meng et al. (2014, 2016) proposed a novel beamforming algorithm using the ZC sequence to achieve omnidirectional radiation pattern in massive multiple-input multiple-output (MIMO) systems. The ZC sequence is a constant amplitude zero autocorrelation (CAZAC) sequence and the Fourier transform of the ZC sequence is also constant-envelop, which meets our requirements perfectly.

Let us define a corrective phase $\phi_{\mathrm{cor},n}$ added to $\phi_{\mathrm{std},n}$. The resultant phase for the n^{th} phase shifter is $\phi_n = \phi_{\mathrm{std},n} + \phi_{\mathrm{cor},n}$, and the beamforming weight for the n^{th} antenna can be written as

$$w_n = w_{\mathrm{std},n} w_{\mathrm{cor},n} = \frac{1}{\sqrt{N}} \mathrm{e}^{\mathrm{j}(\phi_{\mathrm{std},n} + \phi_{\mathrm{cor},n})}. \tag{17}$$

Correspondingly, the revised analog beamforming vector can be expressed as

$$\boldsymbol{w} = \boldsymbol{w}_{\mathrm{std}} \odot \boldsymbol{w}_{\mathrm{cor}}, \tag{18}$$

where

$$\boldsymbol{w}_{\mathrm{cor}} = \left[\mathrm{e}^{\mathrm{j}\phi_{\mathrm{cor},0}}, \mathrm{e}^{\mathrm{j}\phi_{\mathrm{cor},1}}, \ldots, \mathrm{e}^{\mathrm{j}\phi_{\mathrm{cor},N-1}}\right]^{\mathrm{T}}, \tag{19}$$

which denotes the corrective vector for the standard analog beamforming vector $\boldsymbol{w}_{\mathrm{std}}$. By substituting Eq. (19) into Eq. (15), the frequency-domain response $H(f)$ can be rewritten as

$$H(f) = \frac{1}{\sqrt{N}} \sum_{n=0}^{N-1} \mathrm{e}^{\mathrm{j}\phi_{\mathrm{cor},n}} \mathrm{e}^{-\mathrm{j}2\pi n f \frac{d \sin\theta}{c}}. \tag{20}$$

From Eq. (20), we can observe that designing the sequence $w_{\mathrm{cor},n} = \mathrm{e}^{\mathrm{j}\phi_{\mathrm{cor},n}}$ ($n = 0,\ 1,\ \ldots,\ N-1$) can obtain a frequency-flat spatial equivalent channel. Let us define a variable $s = fd\sin\theta/c$ and $s \in [-Bd\sin\theta/(2c),\ Bd\sin\theta/(2c)]$. Then, we sample $H(s)$ uniformly at N points, and obtain the DFT of the corrective weight $w_{\mathrm{cor},n}$ in terms of the antenna index n, which can be expressed as

$$H_k = \frac{1}{\sqrt{N}} \sum_{n=0}^{N-1} \mathrm{e}^{\mathrm{j}\phi_{\mathrm{cor},n}} \mathrm{e}^{-\mathrm{j}2\pi \frac{kn}{N}}, \tag{21}$$

where $k = 0,\ 1,\ \ldots,\ N-1$. Strictly speaking, we should investigate the case in which s varies continuously in $[-Bd\sin\theta/(2c),\ Bd\sin\theta/(2c)]$. Nevertheless, it is reasonable to regard H_k ($k = 0,\ 1,\ \ldots,\ N-1$) as a perfect approximation when N is large. Now we design the sequence $w_{\mathrm{cor},n}$ ($n = 0,\ 1,\ \ldots,\ N-1$) based on the ZC sequence (Chu, 1972), which is written as

$$w_{\mathrm{cor},n} = \begin{cases} \mathrm{e}^{\mathrm{j}\pi \frac{rn(n+2q)}{N}}, & N \text{ is even}, \\ \mathrm{e}^{\mathrm{j}\pi \frac{rn(n+2q+1)}{N}}, & N \text{ is odd}, \end{cases} \tag{22}$$

where parameters r and q are integers and r is relatively prime to N. Taking the derivative of the phase of corrective variable $w_{\mathrm{cor},n}$, we can obtain its frequency range $s \in [rq/N, r(N-1+q)/N]$. Additionally, we know the expected frequency range $s \in [-Bd\sin\theta/(2c),\ Bd\sin\theta/(2c)]$. Then, we can obtain the parameters r and q, given by

$$r = \frac{NBd\sin\theta}{c(N-1)}, \tag{23}$$

$$q = \frac{-(N-1)}{2}. \tag{24}$$

Finally, the corrective phase $\phi_{\mathrm{cor},n}$ is given by

$$\phi_{\mathrm{cor},n} = -\frac{\pi B}{c} nd\sin\theta + \frac{\pi Bd\sin\theta \cdot n^2}{c(N-1)}. \tag{25}$$

An example of the frequency-domain response of the spatial equivalent channel in the proposed ZC-based beamforming method is shown in Fig. 6. We can see that the spatial equivalent channel using the proposed ZC-based beamforming method can effectively eliminate the deep fading points caused by beam squint.

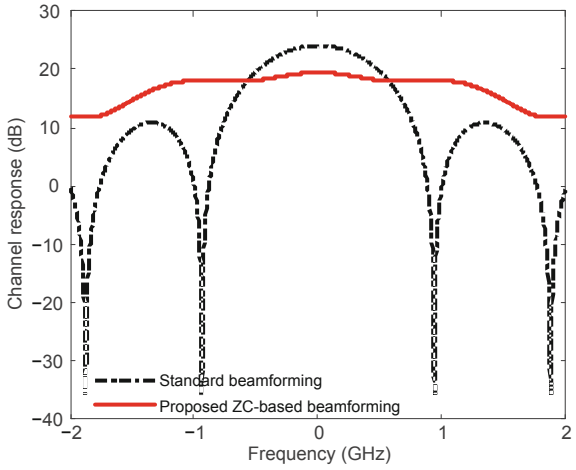

Fig. 6 Frequency-domain response of the spatial equivalent channel in the proposed ZC-based beamforming method ($\theta = 30°$, $N = 256$, $f_c = 60$ GHz)

4 Frequency-domain equalization in mmWave SC-FDE systems

To investigate the beam squint effect on the considered high-throughput mmWave communication system, we view the physical LoS-MISO channel and the analog beamforming as a spatial equivalent channel. As shown in Section 3, the spatial equivalent channel is a frequency-selective channel, in which multiple deep fading points exist. Thus, the RX may see multiple transmitted symbols at a sampling time, and there exists ISI in the above communication channel, causing further deterioration in system performance (except for the beamforming gain loss due to beam squint). In this section, we introduce the equalization algorithms at the RX in the mmWave SC-FDE system to mitigate ISI. In our concerned system scenario, the frequency-domain equalizers (ZF or MMSE) can also be regarded as a digital frequency-domain compensator for mitigating ISI caused by beam squint. Actually, if there is no beam squint, the concerned communication channel is an additive white Gaussian noise (AWGN) channel (only existing noise), and the equalizer at the RX is not essential.

Generally, the mmWave SC-FDE system adopts a block transmission structure. Assume that there are M symbols packed in one block, and that a cyclic prefix (CP) with length M_{CP} is inserted in front of the block which is repetition of the last M_{CP} symbols of the block. A CP is inserted to ensure that the convolution of the transmission block and the channel is circular and to prevent the inter-block interference (IBI), and the length of CP M_{CP} is larger than the delay spread of the channel at least. In our proposed spatial equivalent channel, the delay spread of the channel is $\tau_{\max}$. As mentioned earlier, the worst case delay spread is $\tau_{\max\_\mathrm{worst}} = 4.26T_{\mathrm{sys}}$ in a 60-GHz mmWave system with $N = 256$. Thus, the length of CP is five at least. We can see that beam squint has little effect on the selection of the CP length. In addition, many equalization algorithms are based on symbol-spaced sampling, but the symbol-spaced equalizers are sensitive to the sampling time error. In this study, we prefer fractionally spaced equalization (Yue et al., 2014) to eliminate ISI and compensate for the timing error with a higher sampling rate.

At the RX, we assume that the sampling rate is $f_{\mathrm{s}} = \rho f_{\mathrm{sys}}$, where ρ is the up-sampling ratio (i.e., multiple of symbol rate). Using the sampled data with the CP removed, the $K = \rho M$ point fast Fourier transform (FFT) operation is performed to transform the time-domain sampled data to the frequency domain. Let $\boldsymbol{Y} = [Y(0), Y(1), \ldots, Y(K-1)]^{\mathrm{T}}$ be the frequency-domain data using the FFT operation,

which can be represented as

$$\boldsymbol{Y}=\boldsymbol{H}\boldsymbol{S}+\boldsymbol{N}, \tag{26}$$

where $\boldsymbol{S}=[S(0),S(1),\ldots,S(K-1)]^{\mathrm{T}}$ denotes the frequency-domain sampled data of the transmitted signal $s(f)$, $\boldsymbol{N}=[N(0),N(1),\ldots,N(K-1)]^{\mathrm{T}}$ denotes the frequency-domain noise vector, and $\boldsymbol{H}=\mathrm{diag}(H(0),H(1),\ldots,H(K-1))$ is a diagonal matrix with the diagonal element $H(k)$ representing the discrete frequency response of the spatial equivalent channel at the frequency point f_k. In the K-point FFT operation with the sampling rate f_{s}, the frequency resolution is f_{s}/K and the index k represents a discrete frequency,

$$f_k=\begin{cases}\dfrac{kf_{\mathrm{s}}}{K}, & k=0,\,1,\,\ldots,\,\frac{K}{2}-1,\\ \dfrac{(k-K)\,f_{\mathrm{s}}}{K}, & k=\frac{K}{2},\,\frac{K}{2}+1,\,\ldots,\,K-1.\end{cases} \tag{27}$$

Then, the RX adopts the frequency-domain equalizer $\boldsymbol{G}\in\mathbb{C}^{K\times K}$ to mitigate ISI. The frequency-domain data after equalization are $\boldsymbol{Z}=\boldsymbol{G}\boldsymbol{Y}$. After the inverse FFT (IFFT) operation, the received time-domain data become $\boldsymbol{z}=\boldsymbol{F}^{\mathrm{H}}\boldsymbol{Z}$, where $\boldsymbol{F}$ is the normalized FFT matrix and $\boldsymbol{F}^{\mathrm{H}}$ is the corresponding normalized IFFT matrix. The entries in matrix $\boldsymbol{F}$ are $F_{k,m}=1/\sqrt{K}\cdot\exp(-\mathrm{j}2\pi km/K)$ $(0\le k,\ m\le K-1)$. Finally, the received data $\boldsymbol{z}$ are extracted with a factor of the integer ρ for detection. A simple equalization algorithm is the linear ZF equalization, which is

$$\boldsymbol{G}_{\mathrm{ZF}}=(\boldsymbol{H}^{\mathrm{H}}\boldsymbol{H})^{-1}\boldsymbol{H}^{\mathrm{H}}. \tag{28}$$

However, ZF equalization leads to the enhancement of the noise power, especially when deep fading points occur in the channel. Another more effective equalization algorithm is based on the MMSE criterion, in which $\boldsymbol{G}$ is obtained by solving the MMSE problem

$$\min_{\boldsymbol{G}} E\left[(\boldsymbol{G}\boldsymbol{Y}-\boldsymbol{S})^{\mathrm{H}}(\boldsymbol{G}\boldsymbol{Y}-\boldsymbol{S})\right], \tag{29}$$

and the optimal equalization coefficients of MMSE equalization can be written as

$$\boldsymbol{G}_{\mathrm{MMSE}}=\left(\boldsymbol{H}^{\mathrm{H}}\boldsymbol{H}+\frac{\sigma^2}{P}\boldsymbol{I}\right)^{-1}\boldsymbol{H}^{\mathrm{H}}, \tag{30}$$

where $\boldsymbol{I}$ denotes the identity matrix.

The MMSE equalization algorithm takes the channel noise into account, which overcomes the shortcoming of the ZF equalization algorithm.

The channel state information (CSI) is required at the RX to calculate equalization coefficients with the ZF and MMSE algorithms. In existing SC-FDE systems, the CSI is estimated by inserting the estimation sequence in each frame. For the application scenarios in our work, the spatial equivalent channel has the explicit expression. Thus, as a simple alternative, the channel can be reconstructed at the RX with the AoD of the physical LoS-MISO channel, and the system spectral efficiency can be further improved using the reconstructed channel.

5 Simulation results

In this section, we present BER simulation results to illustrate the beam squint effect on a high-throughput mmWave SC-FDE system with an ultra-massive phased array, and demonstrate the effectiveness of the proposed ZC-based beamforming. The system parameters in simulation are summarized in Table 1. In the simulation, we choose the first antenna as the reference antenna with perfect synchronization at the transceiver. We assume that the AoD of the physical LoS-MISO channel is known perfectly at the transceiver, and there is no quantization loss of the phase shifters in the ultra-massive phased array. Moreover, the BER performance of the optimal TTD-based array or FD array is simulated as a benchmark. These arrays do not have beam squint issues, and the beamforming gain $10\lg N=24.08$ dB can be obtained absolutely.

The BER performance versus SNR is shown in Fig. 7 with $\theta=10°$. Under the above simulation conditions, the spatial equivalent channel is a non-flat channel in which deep fading does not occur, as shown in Fig. 4. It means that the beam

Table 1 Summary of system parameters in simulation

Parameter	Value
Carrier frequency f_{c} (GHz)	60
Carrier wavelength λ_{c} (mm)	5
Transmission bandwidth B (GHz)	4
Modulation	QPSK
Roll-off factor α	0.25
Symbol rate f_{sys} (Gsymbol/s)	3.168
CP length in a symbol block M_{CP}	64
Symbol length in a symbol block M	512
Up-sampling ratio at RX ρ	2
FFT size at RX K	1024
Number of antennas N	256
Antenna spacing d	$0.5\lambda_{\mathrm{c}}$ (2.5 mm)

quint does not cause ISI, and that the system performance loss is due only to the beamforming gain loss by beam squint. From Fig. 7, we can see that the ZF and MMSE algorithms have similar performance. Compared with the system performance of the optimal TTD-based array or FD array, the beam squint results in a 3-dB system performance loss. Furthermore, the performance of the ZC-based beamforming method is slightly worse than that of the standard analog beamforming method. This is because the proposed ZC-based analog beamforming will cause additional beamforming gain loss slightly even though it can eliminate the deep fading points. However, in this case, there is no deep fading point in the spatial equivalent channel created using the standard analog beamforming method. So, the advantages of ZC-based analog beamforming cannot be reflected.

Fig. 8 shows the BER performance versus SNR when $\theta = 30°$. In this case, the beamforming loss is about 8 dB caused by beam squint, and the spatial equivalent channel created using the standard analog beamforming is a frequency-selective channel that has multiple deep fading points. From Fig. 8, we can observe that the system performance deteriorates significantly due to the ISI caused by beam squint in the standard analog beamforming method. Using the proposed ZC-based analog beamforming, the spatial equivalent channel is relatively flat and does not have deep fading points. The ISI caused by beam squint is mitigated perfectly. Thus, the performance of the proposed ZC-based analog beamforming method is better than that of the standard analog beamforming method.

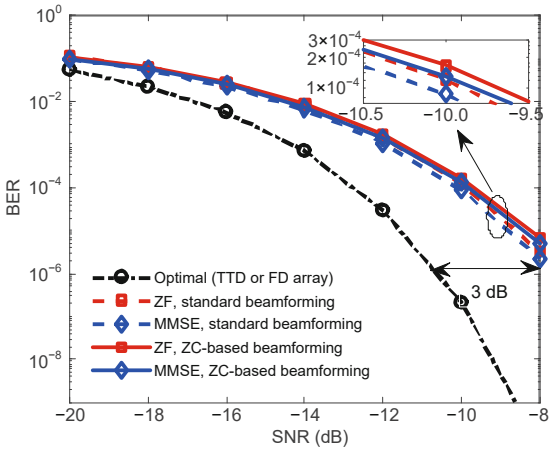

Fig. 7 BER performance versus SNR with $\theta = 10°$

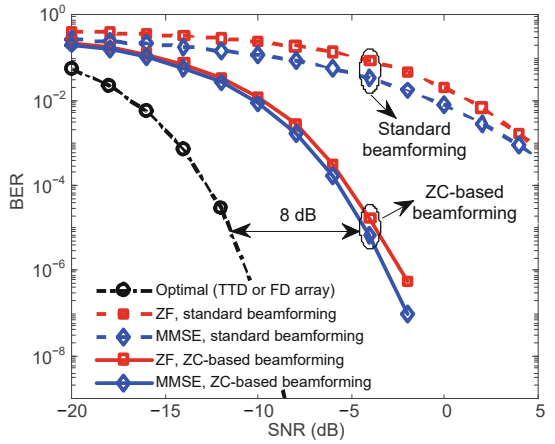

Fig. 8 BER performance versus SNR with $\theta = 30°$

6 Conclusions

In this paper, we have investigated the beam squint effect on a high-throughput mmWave SC-FDE system with an ultra-massive analog phased array. From a communication perspective, the analog beamforming and the physical LoS-MISO channel were viewed as a spatial equivalent channel and the characteristics of spatial equivalent channel were analyzed. To eliminate the deep fading points caused by beam squint, a novel analog beamforming method has been proposed based on the ZC sequence. At the receiver, the frequency-domain equalizer has been designed based on ZF and MMSE criteria. Simulation results demonstrated that the proposed ZC-based analog beamforming can effectively eliminate the beam squint effect on system performance. In future work, we will further study the beam squint effect on mmWave SC-FDE systems in the hybrid analog-digital array architecture and non-light-of-sight (NLoS) channels.

Contributors

Zhiqiang WANG and Guangrong YUE designed the research. Zhiqiang WANG and Jiawei LIU processed the data. Zhiqiang WANG and Guangrong YUE drafted the manuscript. Jun WANG helped organize the manuscript. Zhiqiang WANG, Jiawei LIU, Jun WANG, and Guangrong YUE revised and finalized the paper.

Compliance with ethics guidelines

Zhiqiang WANG, Jiawei LIU, Jun WANG, and Guangrong YUE declare that they have no conflict of interest.

References

Brady JH, Sayeed AM, 2015. Wideband communication with high-dimensional arrays: new results and transceiver architectures. Proc IEEE Int Conf on Communication Workshop, p.1042-1047. https://doi.org/10.1109/ICCW.2015.7247314

Busari SA, Huq KMS, Mumtaz S, et al., 2018. Millimeter-wave massive MIMO communication for future wireless systems: a survey. *IEEE Commun Surv Tutor*, 20(2):836-869. https://doi.org/10.1109/COMST.2017.2787460

Buzzi S, D'Andrea C, Foggi T, et al., 2018. Single-carrier modulation versus OFDM for millimeter-wave wireless MIMO. *IEEE Trans Commun*, 66(3):1335-1348. https://doi.org/10.1109/TCOMM.2017.2771334

Cai MM, Gao K, Nie D, et al., 2016. Effect of wideband beam squint on codebook design in phased-array wireless systems. Proc IEEE Global Communications Conf, p.1-6. https://doi.org/10.1109/GLOCOM.2016.7841766

Chu D, 1972. Polyphase codes with good periodic correlation properties (Corresp.). *IEEE Trans Inform Theory*, 18(4):531-532. https://doi.org/10.1109/TIT.1972.1054840

Falconer D, Ariyavisitakul SL, Benyamin-Seeyar A, et al., 2002. Frequency domain equalization for single-carrier broadband wireless systems. *IEEE Commun Mag*, 40(4):58-66. https://doi.org/10.1109/35.995852

González-Coma JP, Utschick W, Castedo L, 2019. Hybrid LISA for wideband multiuser millimeter-wave communication systems under beam squint. *IEEE Trans Wirel Commun*, 18(2):1277-1288. https://doi.org/10.1109/TWC.2018.2890667

Heath RW, González-Prelcic N, Rangan S, et al., 2016. An overview of signal processing techniques for millimeter wave MIMO systems. *IEEE J Sel Top Signal Process*, 10(3):436-453. https://doi.org/10.1109/JSTSP.2016.2523924

Hemadeh IA, Satyanarayana K, El-Hajjar M, et al., 2018. Millimeter-wave communications: physical channel models, design considerations, antenna constructions, and link-budget. *IEEE Commun Surv Tutor*, 20(2):870-913. https://doi.org/10.1109/COMST.2017.2783541

Kutty S, Sen D, 2016. Beamforming for millimeter wave communications: an inclusive survey. *IEEE Commun Surv Tutor*, 18(2):949-973. https://doi.org/10.1109/COMST.2015.2504600

Liu B, Tan WQ, Hu H, et al., 2018. Hybrid beamforming for mmWave MIMO-OFDM system with beam squint. Proc IEEE 29th Annual Int Symp on Personal, Indoor and Mobile Radio Communications, p.1422-1426. https://doi.org/10.1109/PIMRC.2018.8580998

Liu W, Weiss S, 2010. Wideband Beamforming: Concepts and Techniques. Wiley, Chichester, UK.

Liu XM, Qiao DL, 2019. Space-time block coding-based beamforming for beam squint compensation. *IEEE Wirel Commun Lett*, 8(1):241-244. https://doi.org/10.1109/LWC.2018.2868636

Mailloux RJ, 2005. Phased Array Antenna Handbook (2nd Ed.). Artech House, Boston, USA.

Meng X, Xia XG, Gao XQ, 2014. Constant-envelope omni-directional transmission with diversity in massive MIMO systems. Proc IEEE Global Communications Conf, p.3784-3789. https://doi.org/10.1109/GLOCOM.2014.7037397

Meng X, Gao XQ, Xia XG, 2016. Omnidirectional precoding based transmission in massive MIMO systems. *IEEE Trans Commun*, 64(1):174-186. https://doi.org/10.1109/TCOMM.2015.2498159

Rodriguez-Fernandez J, Gonzalez-Prelcic N, 2018. Channel estimation for frequency-selective mmWave MIMO systems with beam-squint. Proc IEEE Global Communications Conf, p.1-6. https://doi.org/10.1109/GLOCOM.2018.8647269

Roh W, Seol JY, Park J, et al., 2014. Millimeter-wave beamforming as an enabling technology for 5G cellular communications: theoretical feasibility and prototype results. *IEEE Commun Mag*, 52(2):106-113. https://doi.org/10.1109/MCOM.2014.6736750

Rotman R, Tur M, Yaron L, 2016. True time delay in phased arrays. *Proc IEEE*, 104(3):504-518. https://doi.org/10.1109/JPROC.2016.2515122

Sun S, Rappaport TS, Heath RW, et al., 2014. MIMO for millimeter-wave wireless communications: beamforming, spatial multiplexing, or both? *IEEE Commun Mag*, 52(12):110-121. https://doi.org/10.1109/MCOM.2014.6979962

Swindlehurst AL, Ayanoglu E, Heydari P, et al., 2014. Millimeter-wave massive MIMO: the next wireless revolution? *IEEE Commun Mag*, 52(9):56-62. https://doi.org/10.1109/MCOM.2014.6894453

Tse D, Viswanath P, 2005. Fundamentals of Wireless Communication. Cambridge University Press, Cambridge, UK.

Wang ZD, Ma XL, Giannakis GB, 2004. OFDM or single-carrier block transmissions? *IEEE Trans Commun*, 52(3):380-394. https://doi.org/10.1109/TCOMM.2004.823586

Wang ZQ, Cheng L, Wang J, et al., 2018. Digital compensation wideband analog beamforming for millimeter-wave communication. Proc IEEE 87th Vehicular Technology Conf, p.1-5. https://doi.org/10.1109/VTCSpring.2018.8417590

Wu M, Wübben D, Dekorsy A, et al., 2016. Hardware impairments in millimeter wave communications using OFDM and SC-FDE. Proc 20th Int ITG Workshop on Smart Antennas, p.1-8.

Yue GR, Dong AX, Hong H, et al., 2014. Fractionally spaced equalization algorithms in 60GHz communication system. *China Commun*, 11(6):23-31. https://doi.org/10.1109/CC.2014.6879000